Neues Jahrbuch für Mineralogie

Begründet 1807

Abhandlungen

Band 165 · Mit 144 Abbildungen und 53 Tabellen im Text und 1 Beilage

E. Schweizerbart'sche Verlagsbuchhandlung
(Nägele u. Obermiller) · Stuttgart 1993

Printed in Germany.

Calwer Druckzentrum GmbH

Neues Jahrbuch Miner. Abh.	165	3	245–266	Stuttgart, August 1993

Ordering of Fe and Mg in the tourmaline crystal structure: The correct formula

By

Joel D. Grice and **T. Scott Ercit,** Ottawa

With 12 figures and 5 tables in the text

GRICE, J. D. & ERCIT, T. S.: Ordering of Fe and Mg in the tourmaline crystal structure: The correct formula. – Neues Jahrbuch Miner. Abh. **165:** 245–266; Stuttgart 1993.

Abstract: Twelve tourmaline specimens spanning the entire range of Fe–Mg substitution were analyzed by electron microprobe and crystal-structure refinement to determine partitioning of these elements into the 2 octahedral sites, *Y* and *Z*. For each specimen the empirical formula, cell parameters, atomic coordinates, mean bond lengths, atomic site occupancies and bond-valence sums are given. Disorder of Mg between the *Y* and *Z* sites of the tourmaline structure is relatively common for many compositions and significantly complicates formula calculation. To enable formula calculation in the absence of detailed structural information, structural-compositional correlations were sought. A good correlation exists between the partitioning behaviour of Mg and total Fe/(Fe+Mg), i.e. $Mg(Y) \simeq 3\,[1 - Fe/(Fe+Mg)]$, but the *Y*-site Mg content can only be reliably calculated with this equation for compositions with FeO(total) greater than 7 wt.%. However, the Mg content at the *Z* site (and by deduction, at the *Y* site) can be calculated for all compositions from the chemical composition and unit cell volume (*V*) by: $^{Z}[Mg/(Mg+Al)] = 0.209\,\{\exp[(V\text{-}1540)/40] - 1\}$. The substitutions of Ti^{4+} and B for Si and of OH and F for O are discussed. The method of calculation for the correct empirical formula of a tourmaline is given.

Introduction

The crystal structure of tourmaline was first correctly solved by ITO & SADANAGA (1951). Subsequent structure refinements of the various tourmaline species include: dravite (BUERGER et al., 1962), buergerite (BARTON, 1969), elbaite (DONNAY & BARTON, 1972), schorl (FORTIER & DONNAY, 1975), uvite (SCHMETZER et al., 1979), liddicoatite (NUBER & SCHMETZER, 1981). Al-rich elbaite (olenite) (GORSKAYA et al., 1982), feruvite (GRICE & ROBINSON, 1989) and povondraite (GRICE et al., 1993). At present the only species of tourmaline for which there is no structure refinement is chromdravite (RUMANTSEVA, 1983), but NUBER & SCHMETZER (1979) have refined the structure of a Cr-rich dravite.

During the crystal-structure refinements of feruvite and povondraite it became apparent that Fe and Mg do not follow previous assumptions for site partitioning, i.e. Mg and Fe^{2+} at the larger *Y* site and Al^{3+} and Fe^{3+} at the smaller *Z*

0077-7757/93/0165-0245 $ 5.50

site. The first exception to these assumptions was the determination of Fe^{3+} in the *Y* site of buergerite (BARTON, 1969). FORTIER & DONNAY (1975) refined the crystal structure of schorl, assigning Fe^{3+} and Fe^{2+} to the *Y* site and Fe^{2+} to the *Z* site, but on the basis of questionable interpretation of ^{57}Fe-Mössbauer data (HERMON et al., 1973).

In order to resolve the problem of Fe and Mg substitution in tourmaline, 12 specimens were chosen from approximately 50 analyzed samples which span the entire range of Fe and Mg compositions in the tourmaline group. Care was taken to select specimens with a minimum amount of Ti, Mn, V, Zn and Cr.

Chemical composition

The 12 specimens used in this work are listed in Table 1. In all cases, the crystal used in the structure refinement was subsequently chemically analyzed. The sample of schorl from Cross Lake, Manitoba was analyzed at the University of Manitoba with a MAC 5 electron microprobe using a Kevex energy-dispersion (ED) spectrometer and MAGIC V software. Operating conditions were 15 kV, 10 nA (measured on synthetic fayalite), point-focus beam, 100 s collection time. ED data were corrected for voltage and current drift, and line overlaps were corrected by non-iterative spectral stripping techniques. Standards were: synthetic fayalite (Fe, Si), YAG (Al), willemite (Zn), MnF_2 (Mn), $NaInSi_2O_6$ (Na), chromite (Mg). All other samples were analyzed at the Canadian Museum of Nature with a JEOL model 733 electron microprobe using Tracor-Northern 5500 and 5600 automation and TASK software. These wavelength-dispersion analyses used an operating voltage of 15 kV, a beam current of 25 nA, and a beam diameter of 10 μm. The following standards were used: synthetic gehlenite (Ca, Al), synthetic fayalite (Fe), almandine (Si, Mg, Fe), sodic amphibole (Na), riebeckite (F), synthetic tephroite (Mn), titanite (Ti),

Table 1. Tourmaline samples used in this study.

Sample No.	Mineral Species	Specimen No.	Locality
1	povondraite	144,478	San Francisco mine, Villa Tu nari, Bolivia
2	schorl	2,672	Silver Crater, Hastings Co., Ontario, Canada
3	schorl	49,356	York River, Hastings Co., Ontario, Canada
4	schorl	CROSS	Cross Lake, Manitoba, Canada
5	buergerite	43,293	Mapimi, Durango, Mexico
6	feruvite	53,776	Cuvier Island, New Zealand
7	dravite	43,167	Moctezuma, Sonora, Mexico
8	dravite	32,008	Bronson Station, Hastings Co., Ontario, Canada
9	dravite	43,873	Pierrepont, St. Lawrence Co., New York, USA
10	dravite	43,230	Yinnietharra, Western Australia
11	uvite	52,210	Gouverneur, St. Lawrence Co., New York, USA
12	elbaite	55,224	Minas Gerais, Brazil

All specimens are from the Canadian Museum of Nature, except povondraite (Smithsonian Institution, specimen No. 144,478).

VP_2O_7 (V), sanidine and microcline (K). Vanadium was measured with a LiF crystal so as to avoid potential Ti–V overlap. The Li analyses were by ICP–AES on samples of 300–400 mg. Powder infrared absorption spectra were collected for five samples using a Boem MB 120 FTIR equipped with a diamond-anvil microsample cell. Crystals were crushed in the cell, minimizing the amount of adsorbed water.

The chemical analyses are given in Table 2. The calculation of the number of cations in Table 2 from the electron-microprobe and ICP-AES data is not a straightforward operation as it involves three unknown quantities: the OH content, the B_2O_3 content and the valence state of Fe. With the information derived from the crystal structure analysis these quantities can be derived in the following manner: (1) the anion sum is fixed, O+OH+F = 31 with the OH

Table 2. Chemical composition of tourmaline samples.

	Pov 144,478	Sch 2,672	Sch 49,356	Sch Cross	Brg 43,293	Fuv 53,776	Drv 43,167	Drv 32,008	Drv 43,873	Drv 43,230	Drv 52,210	Elb 55,224
SiO_2	30.74	32.73	33.58	33.97	32.92	33.13	34.04	35.34	35.27	36.42	36.27	36.50
SiO_2	0.00	2.87	1.63	–	0.54	2.19	0.39	0.39	0.52	0.95	0.45	0.00
B_2O_3*	9.17	9.47	10.36	10.36	10.14	10.38	10.83	10.27	10.33	10.99	10.52	11.56
Al_2O_3	1.40	16.26	30.62	31.22	30.70	23.38	27.33	27.42	26.69	31.98	28.05	40.07
V_2O_3	0.04	0.16	0.00	–	0.00	0.00	0.00	0.00	0.00	0.00	0.00	0.00
Fe_2O_3	43.89	14.78	0.86	5.17	12.37	5.44	7.63	4.81	5.46	0.26	0.12	0.00
FeO	2.69	11.24	12.65	9.89	5.98	8.66	4.91	3.45	2.20	0.24	0.00	0.22
MnO	0.00	0.10	0.06	0.56	0.11	0.07	0.00	0.10	0.00	0.00	0.00	3.07
ZnO	–	–	–	1.24	–	–	–	–	–	–	–	–
MgO	6.45	4.66	2.69	0.67	0.16	7.80	7.34	9.28	10.77	11.31	14.24	0.00
CaO	0.00	0.04	0.00	0.00	0.20	3.30	0.99	1.92	1.67	0.50	3.07	0.20
Na_2O	2.12	2.71	2.84	1.44	2.49	1.16	2.35	1.66	2.15	2.62	1.31	2.15
K_2O	1.04	0.19	0.06	–	0.07	0.05	0.00	0.00	0.05	0.00	0.00	0.00
Li_2O	–	0.005	0.032	0.13*	0.000	–	0.005	0.058	0.003	0.003	0.009	1.607
H_2O*	2.56	2.94	2.96	3.15	1.15	3.10	3.18	2.84	2.92	3.31	2.87	3.13
F	0.00	0.00	0.34	–	1.32	0.00	0.00	0.83	0.79	0.34	1.31	1.24
–O = F	0.00	0.00	0.14	0.00	0.56	0.00	0.00	0.35	0.33	0.14	0.55	0.52
	100.10	98.16	98.82	97.80	98.70	98.66	99.00	98.72	99.15	99.06	98.77	100.27
						Unit Cell Contents						
Si	5.94	6.01	5.80	5.90	5.83	5.77	5.78	5.98	5.94	5.90	5.99	5.82
Ti	0.00	0.40	0.21	–	0.07	0.29	0.05	0.05	0.07	0.12	0.06	0.00
B	3.06	3.00	3.09	3.10	3.10	3.12	3.17	3.00	3.00	3.08	3.00	3.18
Al	0.32	3.52	6.24	6.39	6.41	4.80	5.47	5.47	5.29	6.11	5.46	7.53
V^{3+}	0.01	0.02	0.00	–	0.00	0.00	0.00	0.00	0.00	0.00	0.00	0.00
Fe^{3+}	6.38	2.04	0.11	0.68	1.65	0.71	0.98	0.61	0.69	0.03	0.02	0.00
Fe^{2+}	0.43	1.73	1.83	1.44	0.89	1.26	0.70	0.49	0.31	0.03	0.00	0.03
Mn	0.00	0.02	0.01	0.08	0.02	0.01	0.00	0.01	0.00	0.00	0.00	0.41
Zn	–	–	–	0.16	–	–	–	–	–	–	–	–
Mg	1.86	1.28	0.69	0.17	0.04	2.03	1.86	2.34	2.70	2.73	3.51	0.00
Ca	0.00	0.01	0.00	0.00	0.04	0.62	0.18	0.35	0.30	0.09	0.54	0.03
Na	0.79	0.96	0.95	0.49	0.86	0.39	0.77	0.55	0.70	0.82	0.42	0.66
K	0.26	0.04	0.01	–	0.02	0.01	0.00	0.00	0.01	0.00	0.00	0.00
Li	–	0.004	0.022	0.09	0.000	–	0.003	0.039	0.002	0.002	0.006	1.03
OH	3.30	3.60	3.41	3.65	1.36	3.60	3.60	3.21	3.28	3.58	3.16	3.33
F	0.00	0.00	0.19	–	0.74	0.00	0.00	0.44	0.42	0.17	0.69	0.62
O	27.70	27.40	27.40	27.35	28.90	27.40	27.40	27.35	27.30	27.25	27.15	27.05

–: not sought, 0.0: not detected, *: calculated by stoichiometry. Pov: povondraite, Sch: schorl, Brg: buergerite, Fuv: feruvite, Drv: dravite, Uvt: uvite, Elb: elbaite.

Table 3. Tourmaline cell dimensions, bond lengths and orientation.

Sample	a (Å)	c (Å)	V (Å³)	⟨X–O⟩ (Å)	⟨Y–O⟩ (Å)	⟨Z–O⟩ (Å)	⟨B–O⟩ (Å)	⟨T–O⟩ (Å)	ΔwR (%)
Povondraite	144,478	16.186(5)	7.444(4)	1,689	2.74	2.04	2.01	1.375	1.621	1.09
Schorl	2,672	16.073(2)	7.306(2)	1,635	2.706	2.059	1.958	1.372	1.620	2.32
Schorl	49,356	15.990(2)	7.195(1)	1,593	2.690	2.045	1.924	1.374	1.623	1.70
Schorl	CROSS	15.972(1)	7.160(1)	1,582	2.698	2.047	1.917	1.373	1.619	–
Buergerite	43,293	15.874(3)	7.196(2)	1,570	2.675	2.004	1.919	1.376	1.619	2.12
Feruvite	53,776	16.000(2)	7.248(1)	1,607	2.654	2.055	1.944	1.375	1.622	–
Dravite	43,167	15.960(4)	7.238(3)	1,597	3.693	2.027	1.938	1.372	1.620	0.30
Dravite	32,008	15.981(1)	7.210(1)	1,595	2.662	2.049	1.929	1.377	1.622	0.76
Dravite	43,873	15.999(3)	7.236(2)	1,604	2.669	2.047	1.935	1.378	1.623	0.58
Dravite	43,230	15.941(2)	7.201(1)	1,585	2.679	2.021	1.927	1.376	1.620	0.10
Uvite	52,210	15.973(3)	7.213(2)	1,594	2.651	2.050	1.929	1.377	1.623	0.15
Elbaite	55,224	15.846(3)	7.119(1)	1,548	2.672	2.019	1.904	1.370	1.618	0.21

content being derived from the bond valence sums (BVS) to O1 and O3, (2) the sum of all cations excluding Na, K and Ca (i.e. *X*-site cations) is 18; the number of B atoms are determined by stoichiometric difference, and (3) Fe^{2+}/Fe^{3+} is determined by charge balance. Understandably it is not practical to do a crystal-structure analysis just to determine a tourmaline formula; consequently, in the Discussion section we present a method for estimation of the correct formula solely from chemical data.

X-ray crystal structure refinements

For the crystal-structure refinements, a sphere (approximately 0.2 mm in diameter) was ground, whenever possible, and the intensity data were collected on a fully automated Nicolet R3m four-circle diffractometer with graphite–monochromatized Mo*Kα* radiation and using the method of Grice & Ercit (1986). Refined cell parameters for each crystal are given in Table 3. The atomic coordinates of feruvite (Grice & Robinson, 1989) were used to begin each refinement and during the final stages of refinement the absolute orientation was checked. Positional parameters and anisotropic temperature factors for each site except H were refined, as were the occupancy parameters of *X*, *Y* and *Z* cation sites. The final positional parameters, equivalent isotropic temperature factors and residuals are given in Table 4. Mean bond lengths are given in Table 3.

Discussion

The structural formula of tourmaline is $XY_3Z_6(BO_3)_3Si_6O_{18}(O, OH, F)_4$. The tourmaline structure (Fig. 1 a), in the acentric space group $R3m$, hosts six-membered rings of SiO_4 tetrahedra. The absolute orientation is exemplified by the fact that all apices of these tetrahedra point in the same direction ($-z$). Barton (1969) established the absolute orientation of the tourmaline structure based on anomalous dispersion; the Fe in buergerite fluoresced strongly with Cu*Kα* X-radiation. Although we used Mo*Kα* radiation, which should produce less anomalous dispersion than Cu*Kα* radiation, the effects are measurable (Table 3) and generally increase in magnitude with Fe content.

Three BO_3 triangles lie parallel to the (001) plane directly above and below the tetrahedral ring. All of the major cation substitutions occur at the three atomic sites *X*, *Y* and *Z* (Fig. 1 b). The *X* site, a nine-fold trigonal antiprism, is centered in the tetrahedral ring while the octahedral sites *Y* and *Z* are just inside and outside the ring, respectively.

In the unit cell of tourmaline there are 31 anions. Of these 27 are oxygen atoms, corresponding to the sites O2 and O4 to O8; the remaining 4 are O, OH or F (1 associated with the O1 site and 3 with O3). With the exception of buergerite, the O3 site hosts only OH, and has a mean bond-valence sum (BVS-

Table 4. Positional and thermal parameters and R Factors.

		Povondraite 144,478	Schorl 2,672	Schorl 49,356	Schorl CROSS	Buergerite 43,293	Feruvite 53,776	Dravite 43,167	Dravite 32,008	Dravite 43,873	Dravite 43,230	Uvite 52,210	Elbaite 55,224
X	x	0	0	0	0	0	0	0	0	0	0	0	0
	y	0	0	0	0	0	0	0	0	0	0	0	0
	z	0.228(2)	0.2301(3)	0.2307(4)	0.2257(6)	0.2154(4)	0.2222(2)	0.2366(6)	0.2271(2)	0.2298(3)	0.2368(3)	0.2291(2)	0.2339(5)
	U_{eq}	273(40)	267(8)	301(11)	298(13)	242(8)	177(4)	241(12)	169(5)	200(6)	214(7)	124(4)	252(11)
Y	x	0.1224(2)	0.12356(3)	0.12375(5)	0.12303(4)	0.13247(4)	0.12299(4)	0.12393(8)	0.12388(5)	0.12427(5)	0.12484(6)	0.12627(7)	0.93857(5)
	y	0.06119(8)	0.06178(2)	0.06187(2)	0.06152(2)	0.06623(2)	0.06149(2)	0.06196(4)	0.06194(2)	0.06214(3)	0.06242(3)	0.06313(3)	0.06143(5)
	z	0.6430(5)	0.63534(9)	0.6326(1)	0.6299(1)	0.6223(1)	0.63661(9)	0.6346(2)	0.6334(1)	0.6336(1)	0.6325(1)	0.6292(1)	0.6298(2)
	U_{eq}	64(8)	90(1)	81(2)	96(2)	119(2)	95(2)	71(4)	76(2)	76(3)	108(3)	75(4)	96(4)
Z	x	0.2987(1)	0.29853(3)	0.29846(5)	0.29827(4)	0.29865(4)	0.29832(3)	0.29810(6)	0.29802(4)	0.29811(4)	0.29795(4)	0.29802(5)	0.29710(5)
	y	0.2627(1)	0.26198(3)	0.26179(5)	0.26162(4)	0.25865(4)	0.26167(4)	0.26164(6)	0.26169(4)	0.26179(4)	0.26162(4)	0.26166(4)	0.26043(5)
	z	0.6124(5)	0.61195(9)	0.6111(1)	0.6105(1)	0.6044(1)	0.6113(1)	0.6122(2)	0.6124(1)	0.6125(1)	0.6121(1)	0.6135(1)	0.6106(1)
	U_{eq}	57(7)	61(2)	48(3)	54(2)	67(2)	67(2)	62(3)	49(2)	52(2)	46(2)	56(2)	66(3)
B	x	0.1097(6)	0.1101(1)	0.1102(1)	0.1102(1)	0.1101(1)	0.1101(1)	0.1099(2)	0.1098(1)	0.1098(1)	0.1098(1)	0.1098(1)	0.1093(2)
	y	0.219(1)	0.2202(2)	0.2203(3)	0.2203(3)	0.2201(2)	0.2200(2)	0.2198(4)	0.2196(2)	0.2197(2)	0.2196(2)	0.2196(2)	0.8907(2)
	z	0.456(2)	0.4554(4)	0.4542(5)	0.4538(5)	0.4523(4)	0.4518(4)	0.4549(8)	0.4531(4)	0.4538(4)	0.4545(4)	0.4524(4)	0.4541(5)
	U_{eq}	86(47)	92(8)	72(10)	82(9)	75(8)	84(8)	90(14)	70(8)	69(9)	63(8)	70(8)	75(10)
Si	x	0.1892(2)	0.19081(3)	0.19184(4)	0.19178(4)	0.19151(4)	0.19151(3)	0.19154(6)	0.19178(3)	0.19173(4)	0.19182(3)	0.19190(3)	0.19196(4)
	y	0.1876(2)	0.18917(3)	0.18998(5)	0.18989(4)	0.19048(4)	0.18985(3)	0.18981(6)	0.19007(4)	0.18998(4)	0.18993(4)	0.19017(4)	0.18989(4)
	z	0	0	0	0	0	0	0	0	0	0	0	0
	U_{eq}	61(10)	64(2)	48(2)	49(2)	54(2)	60(2)	60(3)	47(2)	52(2)	52(2)	52(2)	54(2)
O1	x	0	0	0	0	0	0	0	0	0	0	0	−0.0095(2)
	y	0	0	0	0	0	0	0	0	0	0	0	0.0095(2)
	z	0.772(3)	0.7800(5)	0.7784(7)	0.7809(7)	0.7681(5)	0.7812(5)	0.773(1)	0.7766(5)	0.7748(5)	0.7720(5)	0.7743(4)	0.7818(7)
	U_{eq}	73(44)	202(9)	246(14)	328(14)	181(9)	190(9)	178(16)	156(8)	138(9)	108(8)	97(7)	75
O2	x	0.0609(4)	0.06145(7)	0.06152(9)	0.06181(9)	0.06047(7)	0.0607(1)	0.0613(1)	0.06095(7)	0.06092(8)	0.06098(7)	0.06082(7)	0.06088(9)
	y	0.1219(8)	0.1229(1)	0.1230(2)	0.1236(2)	0.1209(1)	0.1214(1)	0.1226(2)	0.1219(1)	0.1218(2)	0.1220(1)	0.1216(1)	0.93912(9)
	z	0.491(2)	0.4844(3)	0.4836(4)	0.4840(4)	0.4863(3)	0.4764(3)	0.4861(5)	0.4782(3)	0.4798(3)	0.4850(3)	0.4761(3)	0.4856(4)
	U_{eq}	94(33)	108(6)	117(8)	142(7)	90(6)	116(6)	128(10)	101(6)	103(6)	112(6)	95(6)	171(10)
O3	x	0.2578(9)	0.2658(2)	0.2674(2)	0.2682(2)	0.2636(2)	0.2660(2)	0.2635(3)	0.2673(2)	0.2665(2)	0.2644(2)	0.2677(2)	0.2668(2)
	y	0.1289(4)	0.13290(8)	0.1337(1)	0.1341(1)	0.13179(8)	0.1330(1)	0.1318(1)	0.13363(8)	0.13327(9)	0.13219(8)	0.13386(8)	0.1334(1)
	z	0.513(2)	0.5122(3)	0.5114(4)	0.5109(3)	0.5205(3)	0.5125(3)	0.5126(5)	0.5122(3)	0.5123(3)	0.5112(3)	0.5118(3)	0.5095(3)
	U_{eq}	88(34)	138(6)	131(9)	121(8)	90(6)	141(6)	137(12)	111(7)	114(7)	123(7)	105(7)	124(9)

Table 4. (Continued).

		Povondraite 144,478	Schorl 2,672	Schorl 49,356	Schorl CROSS	Buergerite 43,293	Feruvite 53,776	Dravite 43,167	Dravite 32,008	Dravite 43,230	Dravite 43,873	Uvite 52,210	Elbaite 55,224
O4	x	0.0924(4)	0.09252(7)	0.09285(9)	0.09328(8)	0.09452(7)	0.0919(1)	0.0930(1)	0.09254(7)	0.09252(8)	0.09317(8)	0.09232(7)	0.09335(9)
	y	0.1848(8)	0.1850(1)	0.1857(2)	0.1866(2)	0.1890(2)	0.1838(1)	0.1861(3)	0.1851(1)	0.1850(2)	0.1863(2)	0.1847(2)	0.1867(2)
	z	0.069(1)	0.0686(3)	0.0686(3)	0.0682(3)	0.0754(3)	0.0710(3)	0.0696(5)	0.0706(3)	0.0706(3)	0.0700(3)	0.0716(3)	0.0711(3)
	U_{eq}	108(35)	113(6)	97(8)	92(8)	94(7)	114(6)	121(11)	91(6)	96(7)	102(6)	96(6)	93(8)
O5	x	0.1826(8)	0.1835(1)	0.1851(2)	0.1866(2)	0.1823(2)	0.1814(1)	0.1840(3)	0.1828(2)	0.1826(2)	0.1836(2)	0.1820(2)	0.1871(2)
	y	0.0913(4)	0.09174(7)	0.09255(9)	0.09331(9)	0.09116(8)	0.0907(1)	0.0920(1)	0.09140(8)	0.09130(8)	0.09181(8)	0.09100(8)	0.09354(9)
	z	0.087(1)	0.0875(3)	0.0906(3)	0.0901(3)	0.0846(3)	0.0902(3)	0.0904(5)	0.0913(3)	0.0905(3)	0.0914(3)	0.0914(3)	0.0941(3)
	U_{eq}	99(33)	110(6)	95(8)	92(7)	101(7)	111(6)	110(11)	96(6)	98(7)	104(6)	99(6)	98(8)
O6	x	0.1923(5)	0.19557(9)	0.1971(1)	0.1977(1)	0.1928(1)	0.1953(1)	0.1957(2)	0.1962(1)	0.1961(1)	0.1957(1)	0.19604(9)	0.1965(1)
	y	0.1829(5)	0.1864(1)	0.1871(1)	0.1876(1)	0.1865(1)	0.1862(1)	0.1858(2)	0.1869(1)	0.1867(1)	0.1856(1)	0.18700(9)	0.1862(1)
	z	0.784(1)	0.7806(2)	0.7762(2)	0.7759(2)	0.7751(2)	0.7789(2)	0.7783(3)	0.7779(2)	0.7783(2)	0.7768(2)	0.7781(2)	0.7742(2)
	U_{eq}	81(28)	101(5)	85(6)	86(5)	81(5)	98(5)	100(9)	84(5)	88(5)	91(5)	83(5)	83(6)
O7	x	0.2810(5)	0.28323(9)	0.2851(1)	0.2850(1)	0.2868(1)	0.2842(1)	0.2846(2)	0.28486(9)	0.2848(1)	0.2850(1)	0.2850(1)	0.2862(1)
	y	0.2813(5)	0.28328(9)	0.2852(1)	0.2854(1)	0.2860(1)	0.2835(1)	0.2846(2)	0.28434(9)	0.2843(1)	0.28475(9)	0.28433(9)	0.2860(1)
	z	0.075(1)	0.0783(2)	0.0788(3)	0.0785(2)	0.0750(2)	0.0789(2)	0.0791(3)	0.0802(2)	0.0801(2)	0.0790(2)	0.0812(2)	0.0789(2)
	U_{eq}	96(28)	109(4)	85(6)	81(5)	77(5)	105(5)	103(8)	83(5)	91(5)	84(5)	86(5)	75(6)
O8	x	0.2069(5)	0.20850(9)	0.2095(1)	0.2098(1)	0.2095(1)	0.2088(1)	0.2092(2)	0.2095(1)	0.2094(1)	0.2096(1)	0.2097(1)	0.2097(1)
	y	0.2678(5)	0.2696(1)	0.2701(1)	0.2707(1)	0.2700(1)	0.2695(1)	0.2695(2)	0.2702(1)	0.2699(1)	0.2702(1)	0.2702(1)	0.2703(1)
	z	0.442(1)	0.4422(2)	0.4412(3)	0.4408(2)	0.4385(2)	0.4411(2)	0.4416(4)	0.4422(2)	0.4418(2)	0.4410(2)	0.4427(2)	0.4401(2)
	U_{eq}	101(28)	124(5)	95(6)	95(6)	77(5)	123(5)	117(9)	94(5)	101(5)	96(5)	96(5)	87(6)
H1	x		0				0						
	y		0				0						
	z		0.655(8)				0.725(9)						
	U_{eq}*		100				100						
H3	x	0.24(1)	0.255(3)	0.260(3)	0.265(4)		0.258(3)	0.255(4)	0.260(3)	0.262(3)	0.263(3)	0.263(3)	0.265(3)
	y	0.121(7)	0.127(1)	0.130(2)	0.132(2)		0.129(1)	0.127(2)	0.130(1)	0.131(1)	0.131(1)	0.131(1)	0.133(2)
	z	0.41(2)	0.416(4)	0.415(6)	0.416(6)		0.412(4)	0.401(8)	0.409(5)	0.409(5)	0.406(5)	0.403(5)	0.417(6)
	U_{eq}*	100	100	100	100		100	150	100	100	100	100	100
R,	%	5.05	1.43	2.16	1.80	1.77	1.60	2.21	1.75	1.77	1.74	1.79	2.26
wR,	%	5.97	1.77	2.55	2.08	2.11	1.63	2.66	2.14	2.36	2.41	2.18	2.45

* fixed, $R = \Sigma(||Fo| - |Fc||)/\Sigma|Fo|$, $wR = [\Sigma w(|Fo| - |Fc|)^2/\Sigma w|Fo|^2]^{1/2}$, where $w = \sigma^{-2}(Fo)$.

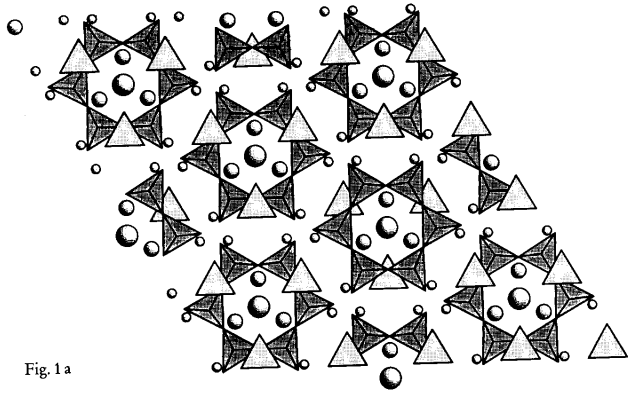

Fig. 1 a

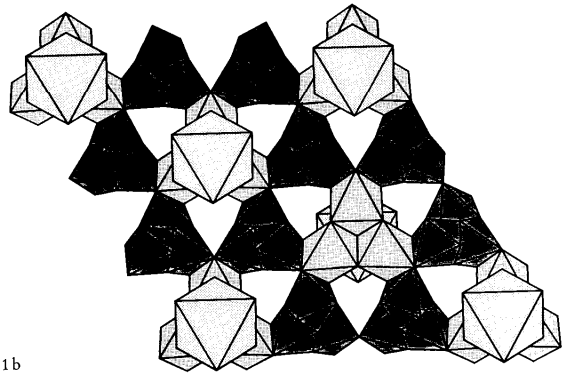

Fig. 1 b

Fig. 1. A [001]-projection of the tourmaline structure showing a) Si tetrahedra and B triangles with the *X*, *Y* and *Z* cations shown as shaded circles (*X* largest, *Z* smallest) and b) *X*, *Y* and *Z* polyhedra with light to dark shading respectively.

calculated from the constants of Brown & Wu, 1976) of 1.14(2) v.u. (Fig. 2). This low mean BVS and small standard deviation indicates that significant H bonding is absent for O3, and that 1.14 v.u. is probably the minimum BVS for O3, i.e. indicating full occupancy by OH or F. For samples with OH at O3,

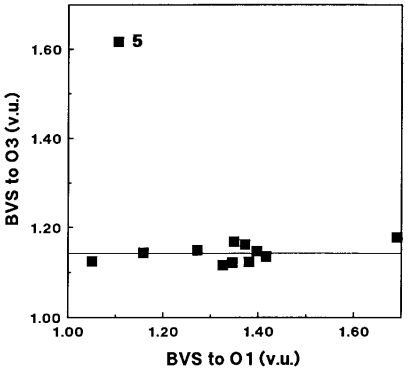

Fig. 2. Plot of bond valence sum of O3 versus O1.

the proton can readily be found from difference Fourier maps (Table 4). For buergerite (sample # 5 in Fig. 2) the BVS to O3 indicates that O, not OH or F is dominant at the site. Further support for this conclusion is in (1) the IR spectrum (Fig. 3) which shows that the OH content of buergerite is low, (2) fully saturated BVS to all non-(OH,F) oxygen sites, which indicates that the high BVS to O3 is not due to strong H bonding to other sites, and (3) although indirect, in the fact that the H atom normally associated with O3 could not be located in the structure refinement of buergerite.

Fig. 2 shows that the BVS to O1 varies considerably, indicating an almost full range (70 %) of substitution of F, OH for O. The minimum observed BVS of 1.05 v.u. indicates (1) that H bonding is not significant for H1, and (2) suggests that the natural minimum BVS for O1 is in the neighbourhood of 1.00 v.u. Fig. 4, a plot of F content versus the BVS to O3, indicates that F variation is independent of the O3 site. Conversely, Fig. 5 shows that F is localized at the O1 site, and that as the F content increases, the BVS to this site decreases. This correlation with the BVS indicates that F⇄O is the dominant substitution at O1; O⇄OH and F⇄OH are of lesser importance. Furthermore, the distribution of data in Fig. 5 suggests the likelihood of end-members with F or O at 01, but not OH.

Given the above relationships, we conclude that the normal assumption of 4(OH,F) per formula unit is not acceptable. OH contents, and by deduction, O contents, at O1 and O3 can be calculated as follows. For O1: OH = 2 – BVS(O1) – F. For O3: OH = [2 – BVS(O3)]/[2 – 1.14].

In all refinements, except for that of elbaite (sample # 12), O1 was found to lie on the 3-fold axis. For elbaite, (1) the high value of U_{eq} (0.035 Å^2) and (2) the

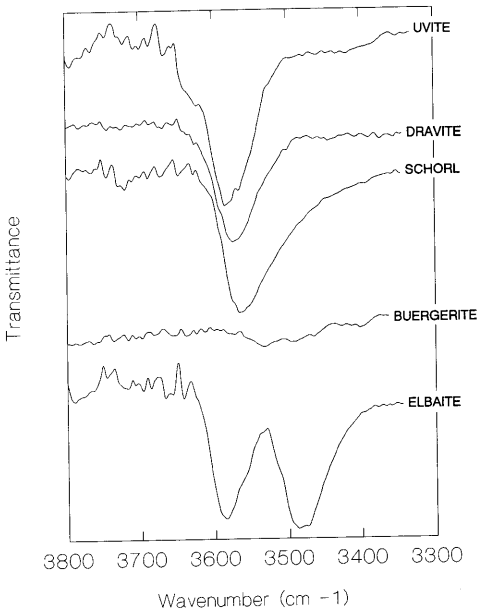

Fig. 3. Infrared spectra of tourmalines.

anisotropy of the displacement parameters, extending in a plane perpendicular to the 3-fold axis indicate that O1 is positionally disordered about the 3-fold axis (Table 4). This displacement fo O1 is probably due to local ordering of Li and Al at *Y*, due to their disparity in size and charge.

Further evidence of local ordering of Li and Al is shown by Fig. 3, IR spectra of five tourmaline samples in the O–H stretching region. All tourmaline samples less elbaite have a single absorption maximum in this region; elbaite differs in having two, well-separated maxima. This behaviour seems to be species-rather than sample-dependent, as comparison to previous compilations indicates (Ferraro, 1982). Given the above structural information for elbaite, interpretation of the splitting of the O–H bands seems relatively straightforward. Some preliminary observations: (1) hydroxyl is much more abundant at O3 than at O1 (approximately 10 times so for elbaite), thus the IR spectra should be dominated by hydroxyl at O3, and (2) OH at both O1 and O3 is not accompanied by significant hydrogen bonding, and the nearest-neighbour en-

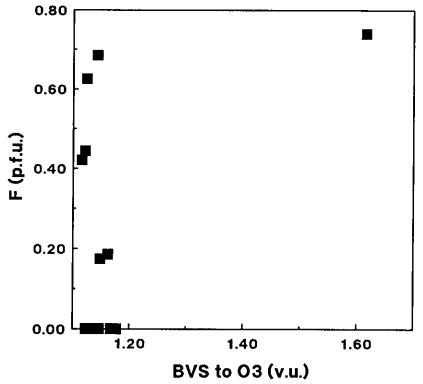

Fig. 4. Plot of number of F atoms per formula unit (p.f.u.) vs. bond valence sum to O3.

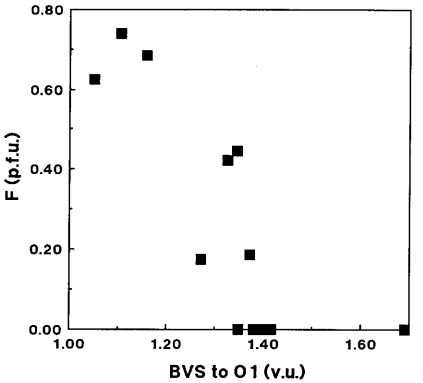

Fig. 5. Plot of number of F atoms p.f.u. vs. bond valence sum to O1.

vironments of O1 and O3 are often similar, thus considerable overlap of O–H bands for O1 and O3 is expected; consequently, (3) interpretation of IR spectra in the O–H stretching region need only involve consideration of O3. For elbaite, as both O1 and O3 are in the coordination sphere of the *Y* site (which hosts Li and Al), local ordering of Li and Al about O1 necessarily results in similar ordering about O3. Li and Al differ sufficiently in electrone-

gativity (1.0 and 1.5, respectively), ionic radius (0.76 and 0.535 Å) and charge that local ordering results in resolution of their respective O–H stretching frequencies into what is essentially a (^{Y}Li^{Z}Al^{Z}Al)OH band at 3580 cm^{-1} and a (^{Y}[Al,Mn]^{Z}Al^{Z}Al)OH band at 3475 cm^{-1}. A shift of this kind (to higher wavenumbers) has been noted for substitution of Li for Al in montmorillonite (Calvet & Prost, 1971).

Fig. 3 shows a shift in the O–H stretching frequency toward lower wavenumbers with progression from uvite to dravite to schorl to buergerite. The band shift corresponds to increasing amounts of substitution of more highly electronegative Fe for less electronegative Mg and Al; i.e., increased substitution of Fe results in more energetic cation-oxygen bonds, thus decreased O–H bond strengths and lower band frequencies. As one would expect from the earlier discussion of bond-valence analysis of the O1 and O3 sites, the effects of F⇄OH substitution upon frequency shifting are of little importance. This is best shown by F-rich uvite 52210 which has the highest principal O–H stretching frequency of all studied samples, whereas it should have one of the lowest frequencies if F⇄OH substitution plays a major role. For all samples the principal stretching frequency is relatively high, which again indicates an absence of significant H bonding in the tourmaline structure.

In the present and previous studies, Si is often observed to be deficient to a small extent (Table 2). Various substitutions have been proposed for this site but the most common suggestion is $Al^{3+} \rightleftarrows Si^{4+}$, coupled with heterovalent substitutions at other sites (Buerger et al., 1962; Foit & Rosenberg, 1979; Foit, 1989). This type of substitution should have the effect of increasing the mean tetrahedral bond length (⟨*T*–O⟩); however, for our data, a positive correlation does not exist between hypothetical ^{IV}[Al] (= 6 – Si) and ⟨*T*–O⟩. More recently, Povondra (1981) suggested Ti⇄Si substitution was significant in tourmaline. It is evident that some of the Si-deficient samples are rich in Ti (Table 2) and have anomalously long *T*–O distances. However, a well developed positive correlation between Ti content and ⟨*T*–O⟩ does not exist for *all* samples. Barton (1969) and Novozhilov et al. (1969) proposed substitution of excess B for Si. However, for our data, the necessary contraction in ⟨*T*–O⟩ accompanying hypothetical ^{IV}[B]⇄Si substitution is not observed. In order to account for deficits in the number of Si atoms per formula unit, yet no systematic increase in either the ⟨*T*–O⟩ distance or in the number of electrons at the Si site, we invoke a model involving substitution of minor amounts of both Ti and B at the Si site for our samples. In order to match the refined number of electrons at the Si site, variable amounts of cations heavier and lighter than Si must be involved; if the relatively large ^{IV}[Ti] represents the heavier cation, then ⟨*T*–O⟩ distances indicate that the lighter cation must be smaller than Si, hence ^{IV}[B] and not ^{IV}[Al]. Fig. 6, the result, shows a relatively good correlation of tetrahedral bond length *versus* mean ionic radius (radii of Shannon, 1976) where any Si deficiencies in the site are first filled by Ti then B.

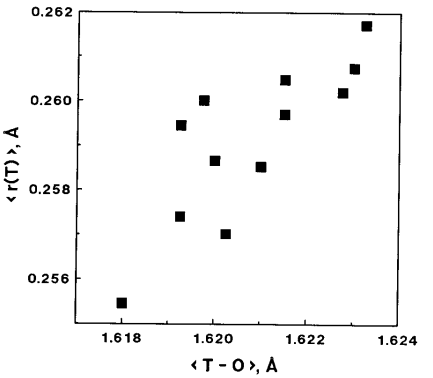

Fig. 6. Plot of mean bond length for the "Si" tetrahedral site vs. arithmetic mean of constituent-ion radii.

For the BO_3 triangle, a small variation in mean bond length was found (1.370 to 1.378 Å); however, scattering data indicate that there is always sufficient B to fill the site and the BVS does not imply any substitutions of other cations. Consequently, the slight variation in ⟨B–O⟩ is inferred to be due to nearest-neighbour effects.

For the *X*, *Y* and *Z* sites linear relationships between the mean bond lengths of the polyhedra and the mean ionic radii of the constituent cations should exist (Hawthorne et al., 1993). Using the ionic radii of Shannon (1976), combined with cation contents derived from the chemical analyses, these relationships are plotted in Fig. 7 for the *X* site (R = 0.920) and in Fig. 8 for a weighted average of the *Y* and *Z* sites (respectively weighted 2 to 1 in accordance with their atomic percentages; R = 0.992). The linearity of the plots attests to the validity of this approach.

The *X* site hosts the large cations Na, Ca and K in the nine-fold coordination of a trigonal antiprism. From Table 5 it can be seen that the sum of the cations at *X* is often low, in agreement with the results from chemical analyses; this alkali deficiency has been noted before (Rosenberg & Foit, 1979; Foit, 1989). The relatively high degree of scatter in Fig. 7 is attributed to the fact that the calculation of mean ionic radii cannot account for the effect of vacancies. For the samples of our study, the *X* site is dominated by Na in nine samples, Ca in two samples, and vacancies in one sample. Due to small sample sizes, K-dominant compositions could not be investigated, although they have been found associated with povondraite (Grice et al., 1993).

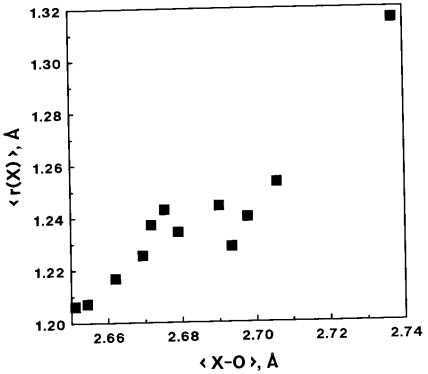

Fig. 7. Plot of mean bond length for the *X* site vs. arithmetic mean of the constituent radii.

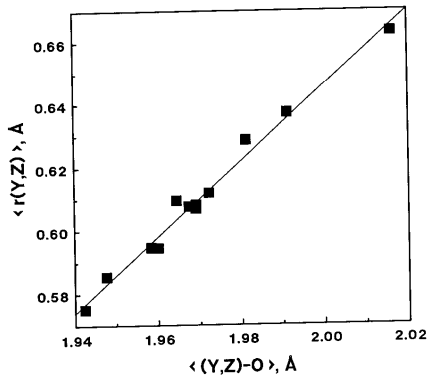

Fig. 8. Plot of weighted-mean bond length for the *Y* and *Z* site octahedra vs. arithmetic means of the constituent-ion raddi.

Although Fig. 8 attests to the merit of the hard sphere model in the correlation of bond length with ionic size for the combined behaviour of the *Y* and *Z* sites, it is of limited practicality. Hence, individual curves for each site were constructed in order to determine the cations present, to assess cation partitioning and to facilitate the calculation of the empirical formulae.

The *Z* site octahedron shows very little variation in BVS (2.85 to 3.03 v.u.) but a considerable range in mean bond length (1.904 to 2.006 Å). Due to the restricted range of BVS, there are few substitutions possible at this site, hence it is relatively easy to predict *Z*-site constituents. The Fe contents of the site are known from refinement of Fe and Al occupancy in the structure refinement (number of electrons in structure, Table 5). As pointed out by HAWTHORNE et al. (1993) the Mg content of this site cannot be determined on the basis of scattering power alone because of the similarity of Mg and Al with respect to X-ray scattering. However, as there is considerable difference in ionic radius between Mg and Al, their proportions can be determined from mean bond lengths. Assignments to the *Y* and *Z* sites were initially made using the curves of HAWTHORNE et al. (1993). However, as our data span a broader compositional range than those of HAWTHORNE et al. (1993), we recalculated the regression curve. Least-squares regression of our data gives: $\langle r(Z)\rangle = 0.94(8)\,\langle Z\text{–}O\rangle - 1.267(3)$ Å; the coefficient of determination (R^2) is 94.3 % (Fig. 9).

The *Y* site octahedron has the most varied cation occupancy in the tourmaline structure and it is at this site that the substitutions critical to determining the formula, and hence the species, take place. Although variation in the mean *Y*–O bond length (2.004 to 2.059 Å) is not as great as in the mean *X*–O or *Z*–O lengths (Table 3), the BVS to the *Y* site varies quite extensively (2.10 to 2.87 v.u.). The *Y* site is assigned the remainder of the Al, Fe^{2+}, Fe^{3+}, Mg (after *Z*-site assignments) and the lesser cations Li, Mn, Zn and V. Fig. 10 shows the fit of these data for the *Y* site calculated on the basis of the remaining cations. Least-squares regression of our data gives $\langle r(Y)\rangle = 1.85(15)\,\langle Y\text{–}O\rangle - 3.065(8)$ Å with $R^2 = 94.3$ %.

Problems exist with povondraite; the data for povondraite do not fit the regressed curves for the *Y* and *Z* sites well (Figs. 9, 10). In particular, the mean radius for the *Z* site is larger than expected, and for the *Y* site, smaller than expected. No simple improvement can be made: (1) the fits have already been maximized by adjusting the amount of Mg disorder between *Y* and *Z*, (2) although addition of Li (not measured for povondraite) would better the agreement between the calculated and observed number of electrons at *Y* (Table 5), it renders a worse fit in Figs. 9, 10. As both the quality of the data and, consequently, the refinement for povondraite were significantly worse than for all other data sets (Table 4), we have assumed that the deviations for povondraite are due to the poorer data quality. Consequently, povondraite was not included in the regression data set.

The lengthy discussions above give the means by which the cations for each site were determined for each of the samples studied. These iterative calculations satisfy the basic crystal chemical properties of charge balance and ionic size. The proof, although indirect, that these are valid principles for tourmaline is the agreement between the calculated and experimentally measured (a) electron scattering power and (b) average bond length at each site. However, the curves of Figs. 8 to 10 are of no practical use in deriving the correct

Table 5. Cation ordering for X, Y, Z and Si sites.

	Pov 144,478	Sch 2,672	Sch 49,356	Sch Cross	Brg 43,293	Fuv 53,776	Drv 43,167	Drv 32,008	Drv 43,873	Drv 43,230	Uvt 52,210	Elb 55,224
X Site												
Ca	0.00	0.01	0.00	0.00	0.04	0.62	0.18	0.35	0.301	0.09	0.54	0.03
Na	0.79	0.96	0.95	0.49	0.86	0.39	0.77	0.55	0.702	0.82	0.42	0.66
K	0.26	0.04	0.01	–	0.02	0.01	0.00	0.00	0.011	0.00	0.00	0.00
	1.05	1.02	0.96	0.49	0.91	1.02	0.95	0.89	1.013	0.91	0.96	0.70
Y Site												
Li	–	0.004	0.022	0.09	0.00	–	0.003	0.039	0.002	0.002	0.006	1.03
Al	0.00	0.00	0.63	0.62	0.91	0.08	0.42	0.00	0.00	0.70	0.00	1.53
Mg	0.05	0.71	0.44	0.17	0.04	1.21	1.40	1.88	2.22	2.23	3.01	0.00
Mn^{2+}	0.00	0.02	0.01	0.08	0.02	0.01	0.00	0.01	0.00	0.00	0.00	0.41
Fe^{2+}	0.43	1.73	1.79	1.21	0.38	1.26	0.21	0.45	0.09	0.03	0.00	0.03
V^{3+}	0.01	0.02	0.00	–	0.00	0.00	0.00	0.00	0.00	0.00	0.00	0.00
Fe^{3+}	2.51	0.52	0.11	0.67	1.65	0.44	0.97	0.61	0.69	0.03	0.02	0.00
Zn	–	–	–	0.16	–	–	–	–	–	–	–	–
	3.00	3.00	3.00	3.00	3.00	3.00	3.00	3.00	3.00	3.00	3.03	3.00
Z Site												
Al	0.32	3.32	5.61	5.77	5.50	4.72	5.05	5.47	5.29	5.41	5.46	6.00
Fe^{3+}	3.88	1.53	0.00	0.23	0.50	0.28	0.49	0.04	0.22	0.00	0.00	0.00
Fe^{2+}			0.04			0.00						
Mg	1.80	0.56	0.25	0.00	0.00	0.82	0.46	0.46	0.48	0.50	0.50	0.00
Ti	0.00	0.40	0.10	–	0.00	0.18	0.00	0.03	0.00	0.09	0.05	0.00
	6.00	6.00	6.00	6.00	6.00	6.00	6.00	6.00	6.00	6.00	6.01	6.00

Table 5. (Continued).

	Pov 144,478	Sch 2,672	Sch 49,356	Sch Cross	Brg 43,293	Fuv 53,776	Drv 43,167	Drv 32,008	Drv 43,873	Drv 43,230	Uvt 52,210	Elb 55,224
Si Site												
Si	5.94	6.01	5.80	5.90	5.83	5.77	5.78	5.98	5.94	5.90	5.99	5.82
Ti	0.00	0.00	0.11	–	0.07	0.10	0.05	0.02	0.06	0.02	0.01	0.00
B	0.06	0.00	0.09	0.10	0.10	0.12	0.17	0.00	0.00	0.08	0.00	0.18
	6.00	6.01	6.00	6.00	6.00	6.00	6.00	6.00	6.00	6.00	6.00	6.00
BVS (Y)	2.80	2.51	2.53	2.53	2.87	2.46	2.56	2.41	2.39	2.41	2.25	2.10
BVS (Y, pred)	2.84	2.18	2.24	2.39	2.85	2.17	2.46	2.19	2.23	2.24	2.00	2.17
BVS (Z)	2.85	2.99	2.93	2.98	3.01	2.86	2.89	2.88	2.87	2.91	2.89	3.03
BVS (Z, pred)	2.70	2.97	2.97	3.00	3.00	2.89	2.92	2.93	2.92	2.93	2.92	3.00
#e (Y, chem)	25.75	22.61	21.04	21.99	21.87	20.01	17.63	16.91	15.62	12.53	12.05	11.01
#e (Y, str)	23.79	22.63	20.83	21.99	22.25	20.16	15.84	16.34	15.73	13.23	12.16	11.43
#e (Z, chem)	21.10	16.81	13.03	13.50	14.08	13.74	13.99	13.05	13.41	13.06	12.99	13.00
#e (Z, str)	21.09	16.61	13.40	13.50	14.08	13.91	14.03	13.17	13.31	12.74	12.84	13.00

See Table 2 for abbreviations and numbering styles. BVS calculated from curves of Brown & Wu (1976).

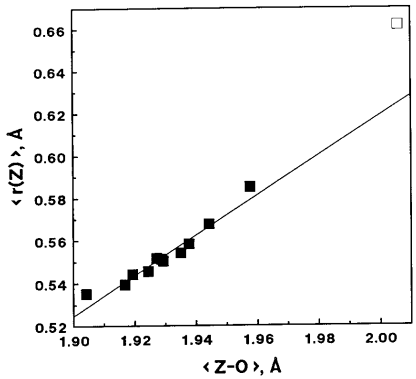

Fig. 9. Plot of calculated vs. observed arithmetic mean of constituent-ion radii for the *Z* site. Hollow square: povondraite.

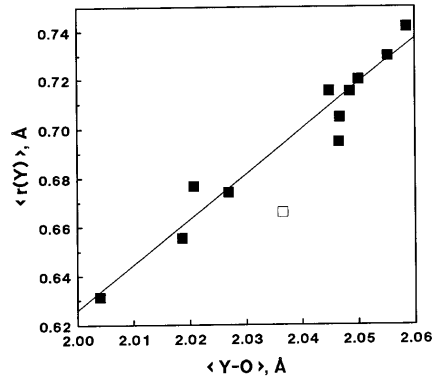

Fig. 10. Plot of calculated vs. observed arithmetic mean of constituent-ion radii for the *Y* site. Hollow square: povondraite.

formula and species designation solely from the chemical composition of a tourmaline. Various structural-chemical relationships were investigated; one of the most useful correlations is presented in Fig. 11, the Mg content of the *Y* site *versus* total Fe/(Fe+Mg). It is evident that solid solution of Fe and Mg at the *Y*

site is almost ideal, i.e. $Mg(Y) \simeq 3\,[1 - Fe/(Fe+Mg)]$. The higher degree of scatter at the Mg-rich end of the plot is due to Mg–Al disorder between the *Y* and *Z* sites. From the point of view of formula calculation, it is fortunate that most tourmalines contain significant amounts of Fe; for compositions with greater than 7 wt.% FeO (total), the line in Fig. 11 could be used to determine

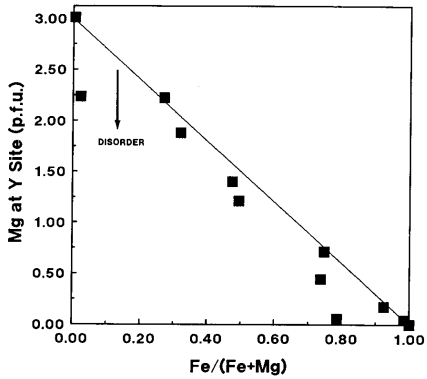

Fig. 11. Plot of the number of Mg atoms at the *Y* site as a function of the Fe/(Fe+Mg) atomic fraction. The line denotes ideal Fe = Mg substitution for ordered Mg.

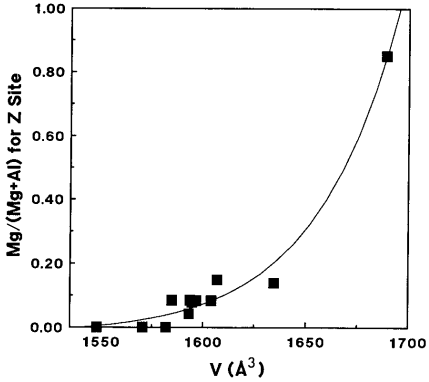

Fig. 12. Plot of Mg/(Mg+Al) for the *Z* site vs. cell colume.

the number of Mg atoms at *Y*, with any remaining Mg assigned to Z. As Fig. 11 uses Fe(total), knowledge of the valence state of Fe is not crucial to making a correct assignment of Mg atoms.

The size of the Z site has the greatest control on cell volume (Foit & Rosenberg, 1979; Foit, 1989). Fig. 12 shows a good correlation between Mg/(Mg+Al) at Z and the unit cell volume. Regression of an exponential model tied to the X-axis at $V = 1540\,Å^3$ gives $^Z[Mg/(Mg+Al)] = 0.209(8)\{\exp[(V-1540)/40] - 1\}$ with $R^2 = 98.4\,\%$. The curve may be of questionable use at the Mg-rich end because of the paucity of data used to model it in this range. However, it serves to estimate Z-site Mg contents well (standard error of estimate = 3 %) over the normal range of tourmaline compositions (dravites, schorls, elbaites and buergerites). As Fig. 12 takes Mg-disorder into consideration, it is preferred over Fig. 11 as a means of estimating the partitioning behaviour of Mg.

Conclusions

This study has led to the recognition of trends indicative of Fe–Mg and Mg–Al disorder in tourmaline. We have been able to determine relationships that resolve the disorder problems such that the correct formula and subsequent species may be derived.

I. The *empirical formula* can be derived from the following procedure:

1. Sum of all cations exclusive of Na, K, Ca (i.e. $Y + Z + Si + B$) = 18.
2. Anion sum = 31 where (a) OH = 3 + (1–F)/2 (an approximation to the data of Fig. 5) and (b) O = 31 – (F+OH).
3. Fe^{2+}/Fe^{3+} derived by charge balance.
4. Si site contains 6 atoms, Si + Ti (added first) + B = 6.
5. *X* site contains Na, K, Ca + site vacancies.
6. *Y* site contains transition metals + Mg, which is estimated by deduction from Fig. 12.
7. Z site contains Al + the remainder of Fe from *Y* + some Mg (estimated from Fig. 12).

II. Some *generalities* that were observed for the crystal chemistry of tourmaline:

1. For uvite or dravite low in Al and with approximately equal numbers of Fe and Mg atoms, the empirical formula is often incorrect if not derived as outlined above.
2. The number of Si atoms is always close to, but often lower than, 6.
3. There is always enough B to fill the trigonal site.
4. The *X* site can be K dominant (Grice et al., 1993), and site-vacancy dominant (schorl sample CROSS).
5. Substitutions at the *Y* site are constrained more by size than valence, hence a large variety of cations is possible: Li, Al, Mg, Fe^{2+}, Fe^{3+}, Mn, V, Zn.
6. Substitutions at the Z site are constrained by valence more than by size, thus fewer cations are involved: Al, Fe^{3+}, Cr and to a lesser extent, Mg.

7. The 31 anions occupy 8 atomic sites. The O3 site tends to be fully occupied by OH, and the O1 site is often partially occupied by F or OH. The remaining sites are all fully occupied by O. The broad IR peak for O–H stretching is split for elbaite due to local ordering of Al and Li at *X*, which causes the OH at the O1 site to be displaced.

Estimation of Li persists as a problem; thus for many compositions of tourmaline, electron microprobe analyses alone are not enough for accurate formula calculation, and will need to be supplemented with the results of other chemical analytical methods, or the results of a structure analysis.

This study emphasizes the importance of crystal structure analysis for determining the systematics of mineral groups. Assumptions as to ionic substitution within complex crystal structures can often be erroneous and should be checked experimentally whenever possible.

Acknowledgements

We are grateful to the following for their cooperation and support in this project: F. C. Hawthorne, University of Manitoba, for use of the single crystal diffractometer; L. A. Groat, University of British Columbia, for collecting two sets of X-ray diffraction data; André Lalonde, University of Ottawa, for Li analyses; R. A. Gault, Canadian Museum of Nature, for performing electron microprobe analyses of several of the samples; R. S. Williams, Canadian Conservation Institute, for collection of infrared spectra. The authors appreciate the constructive reviews by F. F. Foit Jr., an anonymous referee, and editor G. C. Ulmer. The project was funded by a Canadian Museum of Nature, RAC grant.

References

Barton, R., Jr. (1969): Refinement of the crystal structure of buergerite and the absolute orientation of tourmalines. – Acta Cryst. **B 25:** 1524–1533.

Brown, I. D. & Wu, K. K. (1976): Empirical parameters for calculating cation–oxygen bond valences. – Acta Cryst. **B 32:** 1957–1959.

Buerger, M. J., Burnham, C. W. & Peacor, D. R. (1962): Assessment of the several structures proposed for tourmaline. – Acta Cryst. **15:** 583–590.

Calvet, R. & Prost, R. (1971): Cation migration into empty octahedral sites and surface properties of clays. – Clays and Clay Mineral. **19:** 175–186.

Donnay, G. & Barton, R., Jr. (1972): Refinement of the crystal structure of elbaite and the mechanism of tourmaline solid solution. – Tscher. Min. Pet. Mit. **18:** 273–286.

Ferraro, J., ed. (1982): The Sadtler Infrared Spectra Handbook of Minerals and Clays. – Sadtler Res. Labs., Pennsylvania.

Foit, F. F., Jr. (1989): Crystal chemistry of alkali-deficient schorl and tourmaline structural relationships. – Amer. Mineral. **74:** 422–431.

Foit, F. F., Jr. & Rosenberg, P. E. (1979): The structure of vanadium-bearing tourmaline and its implications regarding tourmaline solid solutions. – Amer. Mineral. **64:** 788–798.

Fortier, S. & Donnay, G. (1975): Schorl refinement showing composition dependence of the tourmaline structure. – Can. Mineral. **13:** 173–177.

Gorskaya, M. G., Frank-Kamenetskaya, O. V., Rozhdestvenskaya, I. V. & Frank-Kamenetskii, V. A. (1982): Refinement of the crystal structure of Al-rich elbaite, and some aspects of the crystal chemistry of tourmalines. – Sov. Phys. Cryst. **27** (1): 63–66.

Grice, J. D. & Ercit, T. S. (1986): The crystal structure of moydite. – Can. Mineral. **24:** 675–678.

Grice, J. D., Ercit, T. S. & Hawthorne, F. C. (1993): Povondraite, a redefinition of the tourmaline ferridravite. – Amer. Mineral. **78:** 433–436.

Grice, J. D. & Robinson, G. W. (1989): Feruvite, a new member of the tourmaline group and its crystal structure. – Can. Mineral. **27:** 199–203.

Hawthorne, F. C., MacDonald, D. J. & Burns, P. C. (1993): Reassignment of cation site-occupancies in tourmaline: Al–Mg disorder in the crystal structure of dravite. – Amer. Mineral. **78:** 265–270.

Hermon, E., Simkin, D. J. & Donnay, G. (1973): The distribution of Fe^{2+} and Fe^{3+} in iron-bearing tourmalines: a Mössbauer study. – Tscher. Miner. Pet. Mit. **19:** 124–132.

Ito, T. & Sadanaga, R. (1951): A Fourier analysis of the structure of tourmaline. – Acta Cryst. **4:** 385–390.

Novozhilov, A. I., Voskresenskaya, I. E. & Samoilovich, M. I. (1969): Electron paramagnetic resonance study of tourmalines. – Sov. Phys. Cryst. **14:** 416–418.

Nuber, B. & Schmetzer, K. (1979): Die Glitterposition des Cr^{3+} im Turmalin: Strukturverfeinerung eines Cr-reichen Mg–Al–Turmalins. – N. Jb. Miner. Abh. **137:** 184–197.

– – (1981): Strukturverfeinerung von Liddicoatit. – N. Jb. Miner. Mh. **1981:** 215–219.

Povondra, P. (1981): The crystal chemistry of tourmalines of the schorl–dravite series. – Acta Univers. Carol. Geol. **3:** 223–264.

Rosenberg, P. E. & Foit, F. F., Jr. (1979): Synthesis and characterization of alkali-free tourmaline. – Amer. Mineral. **64:** 180–186.

Rumantseva, E. V. (1983): Chromdravite, a new mineral. – Zap. Vses. Mineral. Obshch. **112:** 222–226 (in Russian).

Schmetzer, K., Nuber, B. & Abraham, K. (1979): Zur Kristallchemie Magnesium-reicher Turmaline. – N. Jb. Miner. Abh. **136:** 93–112.

Shannon, R. D. (1976): Revised ionic radii and systematic studies of interatomic distances in halides and chalcogenides. – Acta Cryst. **A 32:** 751–757.

Manuscript received by the editor June 14, 1992.

Address of the authors:

Mineral Sciences Section, Canadian Museum of Nature, P.O. Box 3443, Station "D", Ottawa, Ontario K1P 6P4, Canada.